Simulation of the Rayleigh-Taylor Instability with the MPS Method

Zhang, Shuai
Department of Applied Quantum Physics and Nuclear Engineering : Graduate Student

Morita, Koji
Institute of Environmental Systems : Associate Professor

Shirakawa, Noriyuki
Institute of Environmental Systems : Professor

Fukuda, Kenji
Institute of Environmental Systems : Professor

出版情報：九州大学工学紀要. 64 (4), pp.215-228, 2004-12. 九州大学大学院工学研究院
バージョン：
権利関係：

Memoirs of the Faculty of Engineering, Kyushu University, Vol. 64, No. 4, December 2004

Simulation of the Rayleigh-Taylor Instability with the MPS Method

by

Shuai ZHANG*, Koji MORITA†, Noriyuki SHIRAKAWA†† and Kenji FUKUDA†††

(Received September 22, 2004)

Abstract

The moving particle semi-implicit (MPS) method is a fully lagrangian particle method for incompressible flow, which is based on particles and their interactions. In this method, grids are unnecessary and a semi-implicit algorithm is used. Using MPS method, the Rayleigh-Taylor instability (RTI) between Silicon oil and water triggered by the buoyancy force is simulated. The results are in consistent with the linear analysis of RTI. The shape of bubbles and spikes obtained in the calculation agrees well with the experimental observations.

Keywords: Moving particle semi-implicit (MPS) method, Rayleigh-Taylor instability (RTI), Particle method

1. Introduction

It is difficult for Eulerian methods to analyze complex geometries and to treat with numerical diffusion caused by fluid convection. Lagrangian methods are other approach to solve these problems, for example a particle-in-cell (PIC) method,[1-2] a smoothing particle hydrodynamics (SPH) method[3-4] and the moving particle semi-implicit (MPS) method.[5-7]

In the PIC method, moving particles simulate the convection directly, which carry the mass, momentum and thermal energy (or entropy). Remaining non-advection terms in the equations are calculated on an Eulerian grid. The information of the particles and gird is transferred back and forth in the calculation with interpolations. As the result, large storage and much computing time are necessary. The other disadvantage is that large implicit diffusion occurs during the interpolation between grid and particles. Though this diffusion can be successfully suppressed in a fluid-implicit-particle method (FLIP), FLIP still needs a grid and brings out other numerical problems.

The SPH method was initially invented to deal with astrophysics problems. It has been developed rapidly in wide variety of areas during the following thirty years. The derivations in SPH are found by analytical differentiation of interpolation formulae without grids. The

*Graduate Student, Department of Applied Quantum Physics and Nuclear Engineering
†Associate Professor, Institute of Environmental Systems
††Professor, Institute of Environmental Systems
†††Professor, Institute of Environmental Systems

momentum and energy equations become sets of ordinary differential equations.

Normally speaking, SPH is a method for compressible flow though it can also solve incompressible flow problems. The MPS method is invented especially to treat the incompressible flow. In the MPS method, the governing equations are discretized with several particle interaction models. These particle interaction models are based on a compact kernel function while models of SPH are derived from the kernel derivatives. A special kernel function is chosen, which prevents particles from clustering. The artificial diffusion terms used in SPH are unnecessary.

A meshless advection using flow-direction local gird (MPS-MAFL) method combines MPS with a gridless method to solve incompressible problems with inlet and outlet.[9-11] Calculation is separated into two steps, that is, a Lagrangian step and an Eulerian step. Convection is directly calculated by moving particles in the Lagrangian step. Using a local grid and rearranging the particles with an arbitrary Lagrangian-Eulerian method (ALE),[12] a new-time physical property at an arbitrary position is obtained.

A two-fluid MPS (T-F MPS) method is developed to solve three-dimensional, multiphase-flow with phase change, which is based on the MPS method. In this method, several new models are presented: surface tension model, heat transfer and phase change model, liquid-gas interface model and buoyancy model.[13-17] Complex flow problems have been successfully solved with this method, for example jet flow[15] and flow around a BWR fuel spacer.[16]

2. MPS Method

2.1 Governing Equations in MPS Method

Governing equations for incompressible flows are the mass, momentum and energy conservation equations as follows:

$$\frac{\partial \rho}{\partial t}+\nabla\cdot(\rho\vec{u})=0 \tag{1}$$

$$\frac{D\vec{u}}{Dt}=-\frac{\nabla p}{\rho}+\nu\nabla^2\vec{u}+\vec{F} \tag{2}$$

$$\rho c_p\frac{DT}{Dt}=\lambda\nabla^2 T-q \tag{3}$$

2.1.1 Kernel Function

For any field $\Phi(\vec{r})$, we consider the delta function

$$\Phi(\vec{r})=\int\Phi(\vec{r}')\delta(\vec{r}-\vec{r}')d\vec{r}' \tag{4}$$

Eq. (4) can be changed using an approximation of the delta function

$$\langle\Phi(\vec{r})\rangle=\int\Phi(\vec{r}')W(\vec{r}-\vec{r}', r_e)d\vec{r}' \tag{5}$$

where $W(\vec{r}-\vec{r}', r_e)$ is an interpolation kernel with the properties

Nomenclature

A	Atwood-number
C_B	tuning parameter of buoyancy
c_p	special heat at constant pressure
d	spatial dimensions
dx	initial distance between two particles
$\vec{F}$	external volume force
$F^{(st)}_i$	surface tension of the particle i
$\vec{g}$	gravity vector
n^0	initial number density
N^0	number of particles within the region of $2dx$ in the initial configuration
N^i	number of particles within the region of $2dx$ in the current configuration
p	pressure
q	energy transfer rate per unit volume
$\vec{r}$	position vector
r_e	cut-off radius of kernel function
$\hat{r}_{ij}$	unit vector from i-particle to j-particle
T	temperature
t	time
$\vec{u}$	velocity vector
W	weight function

Greek symbols

α_1	tuning parameters in the Possion equation
α_2	tuning parameters in the Possion equation
β	definition parameter for free surface
λ	tuning parameters in the diffusion model
λ_c	critical wavelength
λ_m	most unstable wavelength
ρ	density
μ	viscosity
Φ	free energy ratio
ν	kinematic viscosity
Δt	time step size

$$\int W(\vec{r}-\vec{r}', r_e)d\vec{r}=1 \tag{6}$$

and

$$W(\vec{r}-\vec{r}', r_e)\xrightarrow[r_e\to 0]{}\delta(\vec{r}-\vec{r}') \tag{7}$$

In MPS, the kernel function $W(\vec{r}-\vec{r}', r_e)$ is chosen as[6]

$$(\Phi(\vec{r}))_i=\int\Phi(\vec{r})W(\vec{r}-\vec{r}_i, r_e)d\vec{r}\cong\langle\Phi(\vec{r})\rangle_i=\frac{1}{n^0}\sum_{i\neq j}\Phi(\vec{r}_j)w(|\vec{r}_j-\vec{r}_i|, r_e) \tag{8}$$

$$w(|\vec{r}_j-\vec{r}_i|, r_e)=\begin{cases}\left(\dfrac{r_e}{|\vec{r}_j-\vec{r}_i|}\right)-1 & (|\vec{r}_j-\vec{r}_i|<r_e)\\ 0 & (|\vec{r}_j-\vec{r}_i|\geq r_e)\end{cases} \tag{9}$$

$$n^0=\sum_{j\neq i} w(|\vec{r}_j-\vec{r}_i|, r_e) \tag{10}$$

where r_e is the cut-off radius. In MPS, it is chosen to be $2.1dx$,[6] where dx is the initial distance between two particles. With this kernel function, particle clusters are avoided since the value of kernel function is infinity at $|\vec{r}_j-\vec{r}_i|=0$.

2.1.2 Gradient Model

Assuming two particles i and j which possess scalar quantities ϕ_i and ϕ_j, the gradient between these two particles should be

$$(\nabla\phi)_i=\int\frac{\phi-\phi_i}{|\vec{r}-\vec{r}_i|^2}(\vec{r}-\vec{r}_i)\delta(\vec{r}-\vec{r}_i)d\vec{r} \tag{11}$$

In MPS,

$$(\nabla\phi)_i\cong\langle\nabla\phi\rangle_i=\frac{d}{n^0}\sum_{j\neq i}\frac{\phi_j-\phi_i}{|\vec{r}_j-\vec{r}_i|^2}(\vec{r}_j-\vec{r}_i)w(|\vec{r}_j-\vec{r}_i|, r_e) \tag{12}$$

where d is the number of the space dimension.

Obviously, Eq. (12) can be rearranged as follows:

$$\langle\nabla\phi\rangle_i=\frac{d}{n^0}\sum_{j\neq i}\frac{\phi_j-\phi'_i}{|\vec{r}_j-\vec{r}_i|^2}(\vec{r}_j-\vec{r}_i)w(|\vec{r}_j-\vec{r}_i|, r_e) \tag{13}$$

where $\phi'_i=\min(\phi_j)$ and $j\neq i$.

Eq. (13) is tested to be able to improve numerical stability[5-7]

2.1.3 Laplacian Model

Considering a time-dependent diffusion problem, the equation for ϕ is expressed by

$$\frac{d\phi}{dt}=\nu\nabla^2\phi \tag{14}$$

where ν is the diffusion coefficient. Using the Green's function, which is a solution to the diffusion equation with a delta function source at a point $\vec{r}_i$ and time zero, we can get

$$G(|\vec{r}_j-\vec{r}_i|, t)=\left(\frac{1}{\sqrt{4\pi\nu t}}\right)^d\exp\left(-\frac{|\vec{r}_j-\vec{r}_i|^2}{4\nu t}\right) \tag{15}$$

$$\phi(\vec{r}, t)=\int_{-\infty}^{\infty}\phi(\vec{r}', 0)\left(\frac{1}{\sqrt{4\pi\nu t}}\right)^d\exp\left(-\frac{|\vec{r}_j-\vec{r}_i|^2}{4\nu t}\right)d|\vec{r}'| \tag{16}$$

In MPS, we use the kernel function as the transfer function instead of Guassian function. The variance increase $\Delta\sigma^2$ in a time step Δt is

$$\Delta\sigma^2=2d\nu\Delta t \tag{17}$$

The physical quantity transferred from particle i to j in a time step Δt is

$$\Delta\phi_{i\to j}=\frac{2d\nu\Delta t}{\lambda}\frac{1}{n^0}w(|\vec{r}_j-\vec{r}_i|, r_e)\phi_i \tag{18}$$

where λ is the parameter. Therefore the laplacian model used in the MPS is:[5-7]

$$\langle\nabla^2\phi\rangle_i=\frac{2d}{n^0\lambda}\sum_{j\neq i}[(\phi_j-\phi_i)w(|\vec{r}_j-\vec{r}_i|, r_e)] \tag{19}$$

Since diffusion is a linear process, we can superpose the transferred physical quantity and define the parameter λ with the central limit theorem.

$$\lambda=\frac{\int_V w(|\vec{r}_j-\vec{r}_i|, r_e)|\vec{r}_j-\vec{r}_i|^2 dV}{\int_V w(|\vec{r}_j-\vec{r}_i|, r_e)dV} \tag{20}$$

According to Eq. (19), the Laplacian model developed in MPS is conservative.

2.2 Other Models in MPS Method

2.2.1 Incompressible Model

In Eq. (10), we define a parameter n^0 that is called particle number density in MPS. Since each particle processes the same mass, every particle number density n^* should be constant and equal to n^0. Otherwise, we will define

$$n^*+n'=n^0 \tag{21}$$

where n' is the correction of particle number density. As is the case with the MAC method[18], the followings can be derived:

$$\frac{1}{\Delta t}\frac{n'}{n^0}=-\nabla\cdot\vec{u}' \tag{22}$$

$$\vec{u}'=-\frac{\Delta t}{\rho}\nabla p^{n+1} \tag{23}$$

where $\vec{u}'$ is the velocity correction value and $n+1$ means time step number. As the result, we can get the following Possion equation[5-7]

$$\langle\nabla^2 p^{n+1}\rangle_i=-\frac{\rho}{\Delta t^2}\frac{\langle n^*\rangle_i-n^0}{n^0} \tag{24}$$

Eq. (24) can be solved by the incomplete Cholesky conjugate gradient (ICCG) method. ICCG is robust and fast for the calculation with a large number of particles[6]

2.2.2 Surface Tension Model

There are several ways to derive the surface tension model for the MPS method, for example the continuum surface tension force (CSF) method[9-11], the surface potential model[13-17], etc. The surface tension model developed by Shirakawa is expressed by[13-17]

$$\vec{F}_i^{(st)}=\sum_{j\neq i}^{N}\left[-\frac{\partial\Phi(r)}{\partial r}\hat{r}_{ij}\right]\left(\frac{N^0}{N^i}\right)^2 \tag{25}$$

$$\frac{\partial\Phi(r)}{\partial r}=\begin{cases}-0.9\ m/s^2 & 0<|\vec{r}_j-\vec{r}_i|\leq dx\\ 4.5\ m/s^2 & dx<|\vec{r}_j-\vec{r}_i|\leq 2dx\end{cases} \tag{26}$$

where dx is the initial distance between two particles, $\hat{r}_{ij}$ is the unit vector from i particle to j particle, N^0 and N^i are the number of particles in the region of $2dx$ around the particle i in the initial configuration and in the current one, respectively. The parameters in Eq. (26) are determined experimentally. This model is robust, generic and easy to be applied to three-dimensional systems.

2.2.3 Buoyancy Model

For two-phase flow with gas and liquid interface, a buoyancy model should be considered because it is difficult for the MPS method to calculate the pressure head exactly. Shirakawa developed a buoyancy model as follows:[13-17]

$$\vec{u}'_{\xi,i}=-\frac{\Delta td}{n^0\rho_\xi}\left[\sum_{j\neq i}^{N_{\xi=1}+N_{\xi=2}}\frac{P_j-P_{\xi,i}}{|\vec{r}^*_j-\vec{r}^*_{\xi,i}|^2}(\vec{r}^*_j-\vec{r}^*_{\xi,i})w(|\vec{r}^*_j-\vec{r}^*_{\xi,i}|)-\sum_{j\neq i}^{N_{\xi=1}}\vec{g}(\rho_l-\rho_g)f_{BC_B}w(|\vec{r}^*_j-\vec{r}^*_{\xi,i}|)\right] \quad (27)$$

where the second term in the parenthesis represents the buoyancy term. In Eq. (27), $\xi=1$ is for the liquid particles and $\xi=2$ is for the gas particles. c_B is a parameter to tune the buoyancy, which was determined to be 0.003 based on experiments. The function f_B is formulated as

$$f_B(|\vec{r}_j-\vec{r}_i|)=-\frac{|\vec{r}_j-\vec{r}_i|}{r_e}+1 \quad (28)$$

2.3 Boundary Conditions

2.3.1 Free Surface

The MPS method can clearly describe the free surface with particles. A particle is regarded as on the free surface if its number density satisfies the following condition:

$$\langle n^*\rangle_i<\beta n^0 \quad (29)$$

where the parameter β can be from 0.8 to 0.99, which was verified using the numerical experiments.[6]

2.3.2 Wall Boundary Condition

Wall boundarys are simulated with two layers particles which are fixed.[5] Velocities are always zero at these particles. With these particles, number densities of near wall fluid particles can be correctly calculated. The pressures of wall particles are calculated together with fluid particles in the Possion equation. According to the pressure gradient, near wall fluid particles are repelled from the wall without explicit collision.

2.3.3 Periodic Boundary Condition

The MPS method itself can't solve the flow with inlet and outlet (MPS-MAFL method has overcome this difficulty). However MPS can easily simulate the flow with a periodic boundary condition. For the periodic boundary condition in MPS, particles near the inlet and those near the outlet interact each other.

2.4 Moving Particles

Similar to the MAC method, the MPS method separates the calculation into two stages, an explicit stage and an implicit stage, in each time step. In the explicit stage, particles move with the viscosity and external forces that are explicitly calculated by

$$\vec{u}^*_i=\vec{u}^n_i+\Delta t(\nu\nabla^2\vec{u}^n_i+\vec{g}+\vec{F}^{st}_i) \quad (30)$$

$$\vec{r}^*_i=\vec{r}^n_i+\Delta t\vec{u}^*_i \quad (31)$$

In the implicit stage, the velocity is corrected with Eq. (23) to keep the conservation of

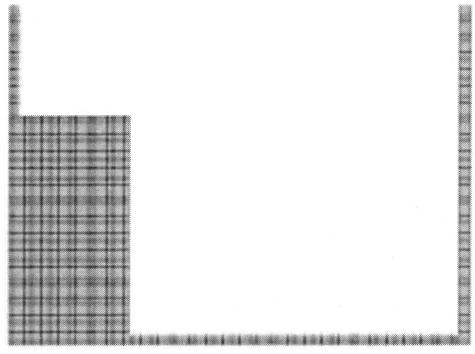

Fig. 1 Initial Configuration of Particles.

the momentum equation. The pressure is obtained with Eq. (24) using the ICCG method. For multi-phase flows, the buoyancy force is added in the pressure gradient using Eq. (27). Normally it needs 10-20 iterations to keep the mass conservation. After that, the energy equation is solved. Then calculation jumps to the next time step.

The dam break problem was chosen to test the code based on the MPS method. The calculation results were compared with the experiment performed by Shirakawa.[13] **Figure 1** shows the initial arrangement of the dam break problem. The water column is 0.2 m in length and 0.4 m in depth. The rectangular vessel is 0.8 m in length, 0.6 m in height and 0.02 m in width. The number of water particles is 3200. The initial distance between two particles is 5×10^{-4} m.

Figure 2 shows the calculation results of the dam break problem. In **Fig. 2**, the particle distributions in the vessel are shown at selected time intervals. They agreed well with the experimental observation.[13] The free surface was clearly represented during all of the time steps. The present results demonstrate that the MPS could be applicable to complex flow problems with free surface.

3. Rayleigh-Taylor Instability

Rayleigh-Taylor instability (RTI) is one of fingering instabilities of an interface between two fluids of different densities, which occurs when the light fluids accelerates the heavy fluid.[21] It occurs in many natural and engineering fields, for example in overturn of the outer portion of the collapsed core of a massive star[22], inertial confinement fusion (ICF) devices[23], etc. There are numerous factors influencing the development of RTI, for example surface tension, viscosity, effects of converging geometry[24] and so on.

As it is known, flunctuations in atomic scale represent "driving forces" of RTI. Molecular Dynamics has successfully simulated RTI using microscopic models.[27] However, this method depends strongly on the computer power available. Classical computational models for RTI needs artificial initial perturbations of the sinusoidal shapes (or the linear combinations of trigonometric functions) instead of spontaneous "driving force".[25-26]

Using the MPS method, Shirakawa has simulated RTI between Silicon oil and water triggered by buoyancy insteadly.[13] One of experimental results is shown in **Fig. 3**, which was also performed by Shirakawa. Calculation results showed that MPS method can qualitively simulate RTI. However, the sharp interface between two liquids was not reproduced reasonably, as can be seen in **Fig. 4**. It may be caused by the boundary conditions defined

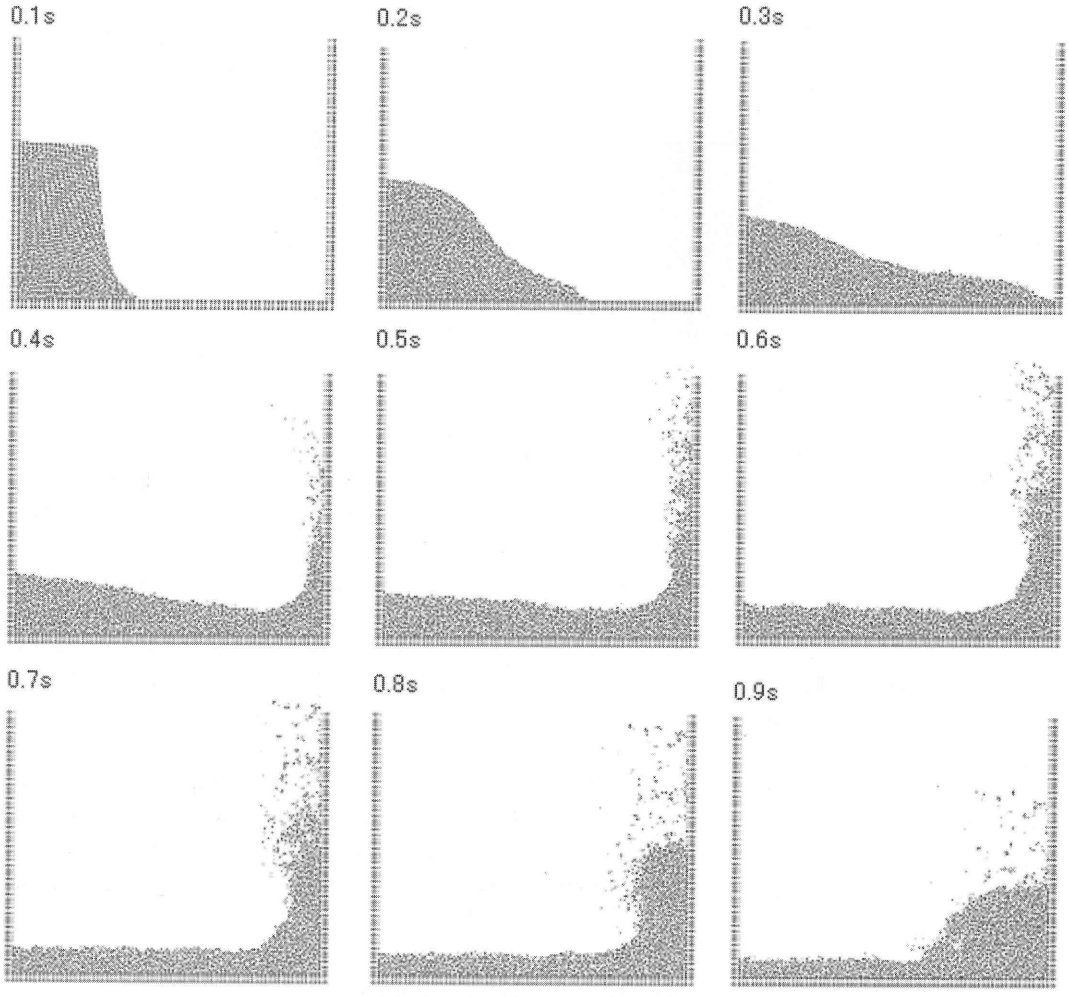

Fig. 2 Calculation Results of the Dam Break Problem.

in the calculation. Ill-chosen boundary conditions in the calculation might lead to the poor result in interface simulation.

In the Shirakawa's simulation, literal and bottom boundaries were set as non-slip walls. In this case, top boundary must be set as free surface. Otherwise, RTI couldn't appear in the simulation. In our calculation, the literal boundary was changed to be periodic. Top and bottom boundaries were set as non-slip walls. Calculation region was 0.1×0.1 m which is the same as Shirakawa's one.

Using the new boundary conditions, Eq. (24) should also be modified since particles were prone to cluster together near the bottom wall. As the result, pressure gradient couldn't be precisely calculated near the wall. In order to overcome this difficulty, a modified Possion equation was derived from the velocity divergence. The equation is expressed by

$$\langle\nabla^2 p^{n+1}\rangle_i=\frac{\rho}{\Delta t}\nabla\cdot\langle\vec{u}^*\rangle_i \tag{32}$$

However Eq. (32) can't prevent particles from clustering. Combining Eq. (24) and Eq.

Fig. 3 Experiment of RTI with the Vessel of 0.4×0.2×0.02 m in Size.

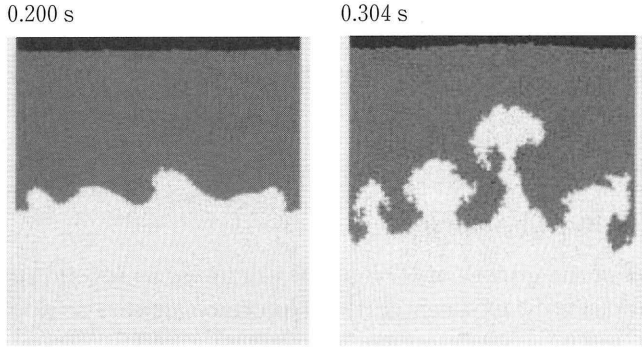

Fig. 4 Calculation Results of RTI by Shirakawa.

(32), we can obtain the following equation:

$$\langle \nabla^2 p^{n+1} \rangle_i = \alpha_1 \frac{\rho}{\Delta t} \nabla \cdot \langle \vec{u}^* \rangle_i - \alpha_2 \frac{\rho}{\Delta t^2} \frac{\langle n^* \rangle_i - n^0}{n^0} \tag{33}$$

and

$$\alpha_1 + \alpha_2 = 1 \tag{34}$$

where α_1 and α_2 are 0.8 and 0.2 respectively in this study. These two coefficients were chosen in consideration of numerical stability.

3.1 Calculation Conditions

The density and kinematic viscosity of Silicon oil are 0.96×10^3 kg/m^3 and 5.0×10^{-5} m^2/s, respectively. Those of water are 1.0×10^3 kg/m^3 and 1.0×10^{-6} m^2/s. Kinematic viscosity between different kind fluid particles is defined as

$$\mu_{ij} = 2\mu_i\mu_j/(\mu_i+\mu_j),\ \nu_i = \mu_{ij}/\rho_i,\ \nu_j = \mu_{ij}/\rho_j \tag{35}$$

The intitial distance between two particles is set to 1.0×10^{-3} m. The surface tension force is calculated for each kind of fluid particle respectively. The bouyancy force is modified for

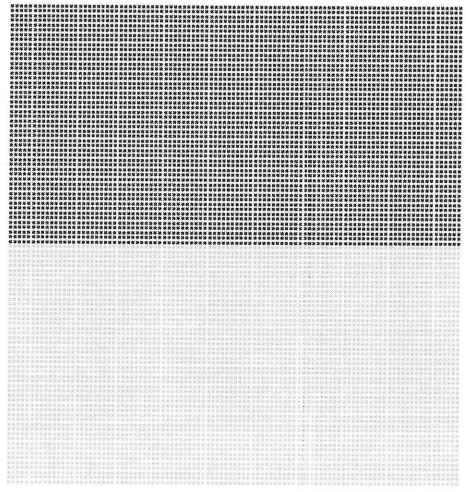

Fig. 5 Initial Arrangement of the Calculation

two liquids flow with the parameter $f_B C_B = 0.75$.[28]

In order to reduce the computational time and storage, the calculation was performed for the flow region of 0.1×0.1 m.

Figure 5 shows the initial arrangement of the RTI simulation. The upper half part the vessel is filled with the water particles and the lower part is the Silicon oil particles.

3.2 Calculation Results and Analysis

The description of the growth of RTI can be organized as several stages.[21] In the first stage, the perturbations grow exponentially and interface appears as ripples. In the calculation results of 0.1 s and 0.2 s, the interface between water and Silicon oil appears as ripples and longer wave disturbances begin to grow rapidly.

In the second stage, the interface grows nonlinearly into the form of bubbles and spikes. In the result of 0.3 s, Silicon oil moves up into the water in the form of round topped bubbles with circular cross sections. Shapes of bubbles and spikes are consistent with the prediction of low Atwood-number RTI.[21] In our calculation the Atwood-number, A, is equal to 0.0204.

In the third stage, the structure on the spikes and interactions among the bubbles will develop into mushroom shapes by the influence of the Helmholtz instability. This effect is more pronounced for RTI with a low Atwood-number. As seen in the result of 0.4 s, the spikes grow into mushroom shapes. So did the shapes of bubbles. It agrees with the experimental observation shown in **Fig. 3** and was similar to the experimental results with low Atwood-number.[29]

According to the linear analysis, surface tension stabilizes perturbations shorter than a critical wavelength

$$\lambda_c = [\sigma / G(\rho_1 - \rho_2)]^{1/2} \tag{36}$$

where ρ_1 and ρ_2 are density of water and Silicon oil separately. σ is the surface tension coefficient between water and Silicon oil. It can be obtained as the following[30]

$$\sigma = \sigma_1 + \sigma_2 - 2\Phi(\sigma_1 \sigma_2)^{1/2} \tag{37}$$

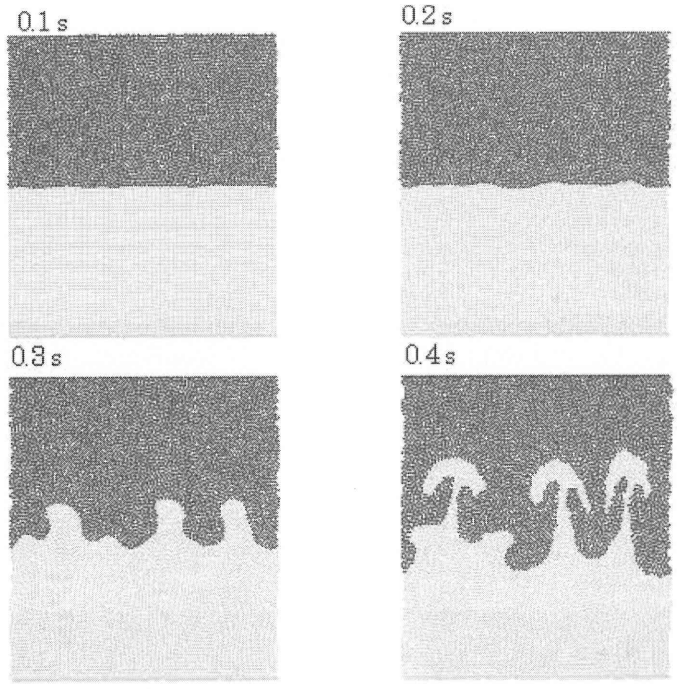

Fig. 6 Calculation Results of RTI.

$$\Phi=\frac{4(V_1V_2)^{1/3}}{(V_1^{1/3}+V_2^{1/3})^2} \tag{38}$$

where σ_1 and σ_2 are surface tension coefficient of water and Silicon oil separately. Φ is the free energy ratio. V_1 and V_2 are molar volume of water and Silicon oil separately.

In our calculation, σ is equal to 0.055 N/m and the critical wavelength is equal to 0.0118 m. Then the fastest growing, or most unstable wavelength is

$$\lambda_m=\sqrt{3}\lambda_c \tag{39}$$

As a result, the value of unstable wavelength is 0.0205 m.

As it is seen in **Fig. 6**, five bubbles growed in 0.3 s. The unstable wavelength was verified to be about 0.02 m. The calculation results are in good agreement with linear theory. On the other hand, though the viscosity isn't taken into consideration, the predition of critical wavelength with the linear theory is exact enough. It means that in our case the voscosity is so small as compared with the surface tension that it can be omitted.

We know that the number of bubbles should be roughly proportional to the geometry size. To verify it, the horizontal size was elongated to 0.15 m. The simulation results are shown in **Fig. 7**. The results can be clearly separated into three stages. The number of bubbles is roughly proportional to the horizontal size. It is worth to note that the interface changes more quickly during the second and third stages. This should be related to the geometry parameters. The aspect ratio was changed from 1 : 1 to 1 : 1.5, which may enhance the non-linear interactions between bubbles and spikes.

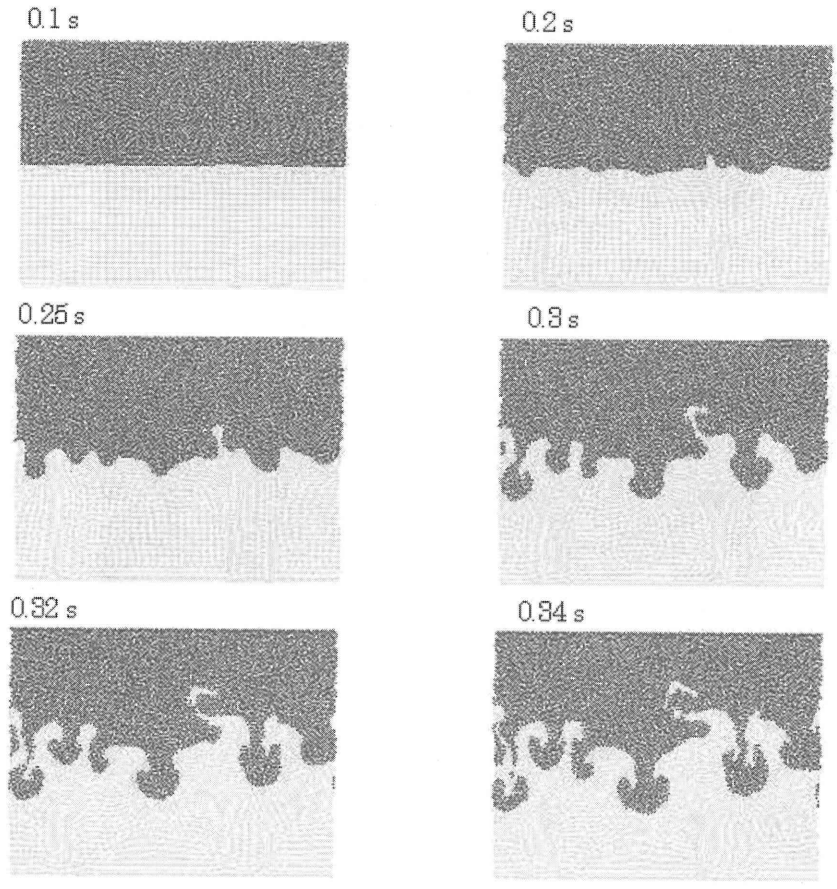

Fig. 7 Calculation Results of RTI in Elongated Calculation Area.

4. Conclusions

A code based on the MPS method has been built to explore its capability of solving complex flow problems. To verify the MPS code, the benchmark calculation of dam break problem was performed to simulate one phase flow with free surface. The simulation results agreed well with the experimental observations. Then the RTI between water and Silicon oil, trigged by buoyancy force, was simulated. The present results showed the typical stages of RTI reasonably and agreed well with the linear analysis. The shapes of bubbles and spikes were consistent with the experimental observations. From above on, we can conclude that the MPS method is a powerful tool to analyze complex flow problems, especially multi-fluid problems that are normally difficult for classic grid methods.

References

1) Francis H. Harlow, PIC and Its Progeny, Computer Physics Communications, 1988, 48, 1-10.
2) Wen Ho LEE, PIC Method for a Two-Dimensional Elastic-Plastic-Hydro Code, Com-

puter Physics Communications, 1988, 48, 11-16.
3) J.J. Monaghan, an Introduction to SPH, Computer Physics Communications, 1988, 48, 89-96.
4) J.J. Monaghan, Smoothed Particle Hydroydynamics, Annu. Rev. Astron. Astrophys, 1992, 30, 543-74.
5) S. Koshizuka, H. Tamako and Y. Oka, a Particle Method for Incompressible Viscous Flow With Fluid Fragmentation, Computational Fluid Dynamics Journal, 1995, 4, 29-46.
6) S. Koshizuka and Y. Oka, Moving-Particle Semi-Implicit Method for Fragmentation of Incompressible Fluid, Nuclear Science and Engineering, 1996, 123, 421-434.
7) Seiichi Koshizuka, Atsushi Nobe and Yoshiaki Oka, Numerical Analysis of Breaking Waves Using the Moving Particle Semi-Implicit Method, Int. J. Numer. Meth. Fluids, 1998, 26, 751-769.
8) J.U. Brackbill, D.B. Kothe and H.M. Ruppel, FLIP: a Low-Dissipation, Particle-In-Cell Method for Fluid Flow, Computer Physics Communications, 1998, 48, 25-38.
9) Han Young Yoon, Seiichi Koshizuka and Yoshiaki Oka, a Particle-Gridless Hybrid Method for Incompressible Flows, Int. J. Numer. Meth. Fluids, 1999, 30, 407-424.
10) Han Young Yoon, Seiichi Koshizuka and Yoshiaki Oka, Direct calculation of Bubble Growth, Departure and Rise in Nucleate Pool Boiling, International Journal of Multiphase Flow, 2001, 27, 277-298.
11) S. Heo, S. Koshizuka and Y. Oka, Numerical Analysis of Boiling on High Heat-Flux and High Subcooling Condition Using MPS-MAFL, International Journal of Heat and Mass Transfer, 2002, 45, 2633-2642.
12) C.W. Hirt, A.A. Amsden and J.L. Cook, an Arbitrary Lagarangian-Eulerain Computing Method for All Flow Speeds, Journal of Computational Physics, 1974, 14, 227-253.
13) Noriyuki Shirakawa, Simulations of Two-Phase Flows and Jet Flows with the Particle Interaction Method, the Ph.D. thesis for the University of Tokyo, 2000.
14) Noriyuki Shirakawa, Hideki Horie, Yuchi Yamamoto and Shigeaki Tsunoyama, Analysis of the Void Distribution in a Circular Tube with the Two-Fluid Particle Interaction Method, Journal of Nuclear Science and Technology, 2001, 38, 392-402.
15) Noriyuki Shirakawa, Hideki Horie, Yuchi Yamamoto, Yaushi Okano and Akira Yamaguchi, Analysis of Jet Flows with the Two-Fluid Particle Interaction Method, Journal of Nuclear Science and Technology, 2001, 38, 729-738.
16) Noriyuki Shirakawa, Yuchi Yamamoto, Hideki Horie and Shigeaki Tsunoyama, Analysis of Flows Around a BWR Spacer by the Two-Fluid Particle Interaction Method, Journal of Nuclear Science and Technology, 2002, 39, 572-581.
17) Noriyuki Shirakawa, Yuchi Yamamoto, Hideki Horie and Shigeaki Tsunoyama, Analysis of Subcooled Boiling With the Two-Fluid Particle Interaction Method, Journal of Nuclear Science and Technology, 2003, 40, 125-135.
18) S. Koshizuka, Computational Fluid Dynamics, Baifukan Co. Ltd., 1999, 123-130.
19) Katsuya Nomura, Seiichi Koshizuka, Yoshiaki Oka and Hiroyuki Obata, Numerical Analysis of Droplet Breakup Behavior Using Particle Method, Journal of Nuclear Science and Technology, 2001, 38, 1057-1064.
20) Ri-Qiang Duan, Seiichi Koshizuka and Yoshiaki Oka, Two-Dimensional Simulation of Drop Deformation and Breakup at Around the Critical Weber Number, Nuclear Engineering and Desigh, 2003, 225, 37-48.
21) D.H. Sharp, an Overview of Rayleigh-Taylor Instability, Physica 12D, 1984, 3-18.
22) R.L. McCrory, L. Montierth, R.L. Morse and C.P. Verdon, Nonlinear Evolution of Ablation of Ablation-Driven Rayleigh-Taylor Instability, Phys. Rev. Lett, 1981, 46,

336-339.
23) L. Smarr and J.R. Wilson, R.T. Barton and R.L. Bowers, Rayleigh-Taylor Overturn in Supernova Core Collapse, Astrophys. J., 1981, 246, 515-525.
24) H.J. Kull, Theory of the Rayleigh-Taylor Instability, Physics Reports (Review Section of Physics Letters), 1991, 206, 197-325.
25) Xiaoyi He, Shiyi Chen and Raoyang Zhang, a Lattice Boltzmann Scheme for Incompressible Multiphase Flow and Its Application in Simulation of Rayleigh-Taylor Instability, Journal of Computational Physical, 1999, 152, 642-663.
26) Andrew W. Cook and Ye Zhou, Energy Transfer in Rayleigh-Taylor Instability, Physical Review, 2002, 66, 1-12.
27) Jacek Moscinski, Witold Alda, Marian Bubak, Witold Dzwinel, Jacek Kitowski, Marek Pogoda and David A. Yuen, Molecular Dynamics Simulations of Rayleigh-Taylor Instability, Annual Review of Computational Physics V, 1997, 97-136.
28) Noriyuki Shirakawa, Private Communication, 2004.
29) M. Ratafia, Experimental Investigation of Rayleigh-Taylor Instability, the Physics of Fluids, 1973, 16, 1207-1210.
30) L.A. Girifalco and R.J. Good, a Theory for the Estimation of Surface and Interfacial Energies. I. Derivation and Application to interfacial, Journal of Physical Chemistry, 1957, Vol.61, 904-909.